ACS Chemical Neuroscience

Research Article

pubs.acs.org/chemneuro

Positron Emission Tomography Imaging of Fibrillar Parenchymal and Vascular Amyloid-β in TgCRND8 Mice

Daniel McLean,[†,‡] Michael J. Cooke,[†] Ricardo Albay, III,[§] Charles Glabe,[§] and Molly S. Shoichet*[,†,‡,∥]

[†]Department of Chemical Engineering and Applied Chemistry, University of Toronto, Toronto, Ontario M5S 3E5, Canada

[‡]Institute of Biomaterials and Biomedical Engineering, University of Toronto, Toronto, Ontario M5S 3G9, Canada

[§]Department of Molecular Biology and Biochemistry, School of Biological Sciences, University of California at Irvine, Irvine, California, United States

[∥]Department of Chemistry University of Toronto, Toronto, Ontario M5S 3H6, Canada

Supporting Information

ABSTRACT: Few quantitative diagnostic and monitoring, tools are available to clinicians treating patients with Alzheimer's disease. Further, many of the promising quantitative imaging tools under development lack clear specificity toward different types of Amyloid-β (Aβ) pathology such as vascular or oligomeric species. Antibodies offer an opportunity to image specific types of Aβ pathology because of their excellent specificity. In this study, we developed a method to translate a panel of anti-Aβ antibodies, which show excellent histological performance, into live animal imaging contrast agents. In the TgCRND8 mouse model of Alzheimer's disease, we tested two antibodies, M64 and M116, that target parenchyma aggregated Aβ plaques and one antibody, M31, that targets vascular Aβ. All three antibodies were administered intravenously after labeling with both poly(ethylene glycol) to enhance circulation and ^{64}Cu to allow detection via positron emission tomography (PET) imaging. We were clearly able to differentiate TgCRND8 mice from wild type controls by PET imaging using either M116, the anti-Aβ antibody targeting parenchymal Aβ or M31, the antivascular Aβ antibody. To confirm the validity of the noninvasive imaging of specific Aβ pathology, brains were examined after imaging and showed clear evidence of binding to Aβ plaques.

Targeting specific forms of amyloid-β with PET compatible radiolabelled antibodies in brains of living animals

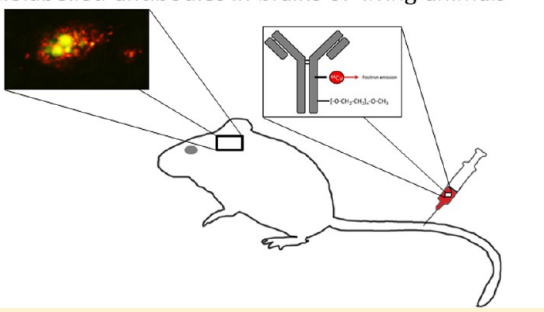

KEYWORDS: *Keyword*

Alzheimer's disease (AD) is an incurable neurodegenerative condition that affects memory and cognition and is most prevalent in individuals over 60 years of age.[1] As the global population experiences increases in longevity, AD is becoming an increasingly relevant disease because it imposes a high economic and social burden.[2,3] Treatment of AD patients is complicated by limited availability of unbiased quantitative diagnostic tools.[4] Two important pathological features of AD, that can be used to develop molecular imaging tools, are accumulation of misfolded amyloid-β (Aβ) species in the extracellular space and intracellular hyperphosphorylation of tau neurofibrillary tangles.[5,6] Most molecular imaging strategies target Aβ because it is an early stage event. Similarly, many promising therapeutics are directed to Aβ and extracellular targets as they are more accessible than intracellular targets.[7−9] Aβ is found in a variety of isoforms which differ in neurotoxicity, and a tool that can target specific types of Aβ is valuable.[10,11]

The most well-known small molecule imaging agent is [*N*-methyl-^{11}C]-2-(4′-methylaminophenyl)-6-hydroxybenzothiazole or conventionally known as ^{11}C-Pittsburgh Compound-B (PIB). PIB is a positron emission tomography (PET) tracer and is classified as a Thioflavin T derivative.[12] PIB is useful because of high penetration of frontal, temporal, parietal, and occipital cortices, but could be problematic because of minimal penetration of the cerebellum and subcortical white matter.[13] False negatives have also been reported with PIB.[14] Small molecules have been successful in detecting Aβ deposits in the brains of humans and are progressing toward clinical use by physicians to diagnose and manage AD; however, none of the major small molecules developed target specific types of Aβ.[15] Synthesizing small molecule tracers with narrow specificity remains challenging. In contrast, production of antibodies with narrow specificity is well established.[16−19]

Antibodies have generated much interest for brain imaging and most efforts have been tailored toward increasing penetration of antibodies to brain tissue. Poduslo and co-workers developed a collection of anti-Aβ conjugates with high brain permeability and excellent Aβ-plaque targeting for use in MRI imaging of

Received: December 11, 2012
Accepted: January 24, 2013
Published: March 19, 2013

transgenic AD mice.[20,21] Koffie et al. reported using poly(*n*-butyl cyanoacrylate) dextran polymers coated with polysorbate 80 nanoparticles (termed PBCA nanoparticles) which can cross the blood-brain barrier and detect Aβ pathology.[22] Notwithstanding these successes, a significant challenge in this field remains developing in vivo imaging techniques that enable detection of anti-Aβ antibodies bound to Aβ in the brain.

Protein adsorption is the first step in clearance of foreign material from the circulation.[23] A common strategy to increase the circulation half-lives of proteins and nanoparticles is to inhibit protein adsorption by coupling to poly(ethylene glycol) (PEG).[24] In addition, PEG is used clinically to increase the half-life of many drugs and is considered to be a biocompatible material.[25,26] By increasing the half-life of our contrast agent, it is expected that higher accumulation in brain tissue will be observed due to the longer circulation time. Further, there is significant evidence that PEG chains can act as a ligand to the cholesterol transport receptors and thereby actively increase accumulation of proteins or nanoparticles in the brain.[27] We have previously shown that PEG-modified 6E10 (a classic anti-Aβ antibody) was able to cross the blood-brain barrier sufficiently to differentiate transgenic TgCRND8 from wild type mice using PET imaging.[28] The positron emitting isotope ^{64}Cu was chelated by DOTA, which was covalently bound to 6E10, thereby allowing PET imaging.

In this study, we aimed to develop techniques that enable the use of a panel of anti-Aβ antibodies to measure different types of Aβ pathology using minimally invasive PET imaging. Three fibril specific conformation-dependent anti-Aβ antibodies (M116, M64, M31), that have shown specificity for aggregated or vascular Aβ, were examined using three sequential screening assays. First, each antibody was characterized ex vivo in TgCRND8 and wild type tissue to demonstrate binding and specificity. Next, the binding, specificity, and elimination of the antibodies were studied in living brain tissue after intracortical injections. Finally, antibodies (modified with ^{64}Cu and PEG) were injected intravenously into animals that were monitored by noninvasive PET imaging over 4 h.

RESULTS AND DISCUSSION

Three strategies were pursued to test anti-amyloid β antibody detection of parenchymal plaques (with M116 and M64) or vascular deposits (with M31) in the brain: (1) antibody binding to ex vivo brain tissue to ensure antibody-plaques binding; (2) direct injection of anti-amyloid β antibodies into the cortex to confirm binding in vivo; and (3) the most clinically relevant, intravenous injection of PEG- and copper-64-modified anti-Aβ antibodies and their detection in the brain by noninvasive PET imaging.

Anti-Amyloid β Antibodies Target Parenchymal Plaques and Vascular Deposits in ex Vivo Brain Tissue. The anti-Aβ antibodies, M116, M64, and M31, were examined for Aβ binding in the ex vivo brain tissue of 5 month old TgCRND8 mice (Figure 1). M116 detects dense deposits (Figure 1A) in the parenchyma of TgCRND8 mice that are Thioflavin S (Thio-S) positive (Figure 1B). The overlaid image (Figure 1C) shows that the core of the M116 positive deposit is composed of Aβ, demonstrating that M116 is a good candidate for imaging Aβ accumulation because of the high binding and low background observed. M64 also detects dense parenchymal deposits (Figure 1D) that are Thio-S positive (Figure 1E). Similarly, the overlay of the M64 and Thio-S images (Figure 1F) shows that the core of the M64 positive deposit is composed of Aβ, indicating that M64 is also a good candidate for in vivo imaging of Aβ pathology; however, the high background observed for M64 may indicate high nonspecific binding in comparison with M116. High nonspecific binding would mask binding to Aβ pathology.

In contrast, M31 did not bind to dense deposits but instead detected hollow circular shapes (Figure 1G) that were similar to the shape of blood vessels. These M31 positive deposits were Thio-S positive (Figure 1H), which confirmed that these deposits were composed of Aβ. Overlay of the M31 and Thio-S images (Figure 1I) showed some colocalization of signal. In order to determine if M31 was indeed binding to vascular deposits of Aβ, tissue sections were stained with CD31, an endothelial-specific antibody that serves as a good marker of blood vessels.[29] A CD31 positive blood vessel (Figure 1J) also stained positive for M31 (Figure 1K). Control tissue was stained without the primary antibody to confirm specificity for the rat primary antibody and no binding to the mouse primary antibody (Figure 1M and N). The overlay of the M31 and CD31 images confirmed the colocalization of these two markers and demonstrated that, in contrast with M116 and M64, M31 is specific to vascular deposits of Aβ. Vascular Aβ burdens are not high at 5 months of age, but previous studies have reported vascular Aβ as early as 3 months of age in TgCRND8 mice.[30] The specific detection of vascular Aβ by M31 confirmed that M31 is a useful candidate for in vivo imaging.

In order to provide some insight into the possible clinical translation of these antibodies, human AD tissue, in Broadmann's area 11, was analyzed with each antibody using histological techniques. Broadmann's area 11 was chosen because high Aβ deposition has been reported in this region of the brain[31] (Figure 2A). M31 (Figure 2B) stained hollow, branched structures, indicating specificity for vascular Aβ deposits, consistent with results in TgCRND8 mouse brain tissue. No similar structures were found when healthy tissue was stained using the same protocol M64 and M116 (Figure 2C, D) which showed affinity for parenchymal Aβ plaques in TgCRND8 mice, stained positive for plaques in human brain tissue. As observed in TgCRND8 mouse brain, M116 exhibited a lower background staining than M64. Binding to Aβ deposits in human tissue suggests that these antibodies may have clinical utility as contrast agents.

Intracortical Delivery of Anti-Amyloid β Antibodies Labels Plaques in the Cortex. In order to demonstrate that the detection of Aβ deposits in a controlled histological environment could be translated to a dynamic in vivo environment, M116, M64, and M31 were injected separately into the cortex of living 5 month old TgCRND8 animals. After allowing the antibodies to diffuse for 4 h, the animals were sacrificed and the brain tissue sectioned and examined using previously developed techniques.[32] Dense deposits similar to those seen histologically were found near the injection site in TgCRND8 mice that received M116 (Figure 3A). In contrast, no M116 positive deposits (Figure 3B) were observed surrounding the injection site in wild type animals that received intracortical injection of M116. Together this provides further evidence that the deposits detected in the TgCRND8 mouse brain are composed of Aβ. Similarly, dense deposits were observed around the injection site in TgCRND8 mice that received intracortical injections of M64 (Figure 3C), while no deposits were found in wild type tissue (Figure 3D). These results confirmed that the detection of Aβ deposits in the parenchyma could be translated from a histological environment to an in vivo environment. M116 or M64 deposits found in TgCRND8 stained positive for Thio-S,

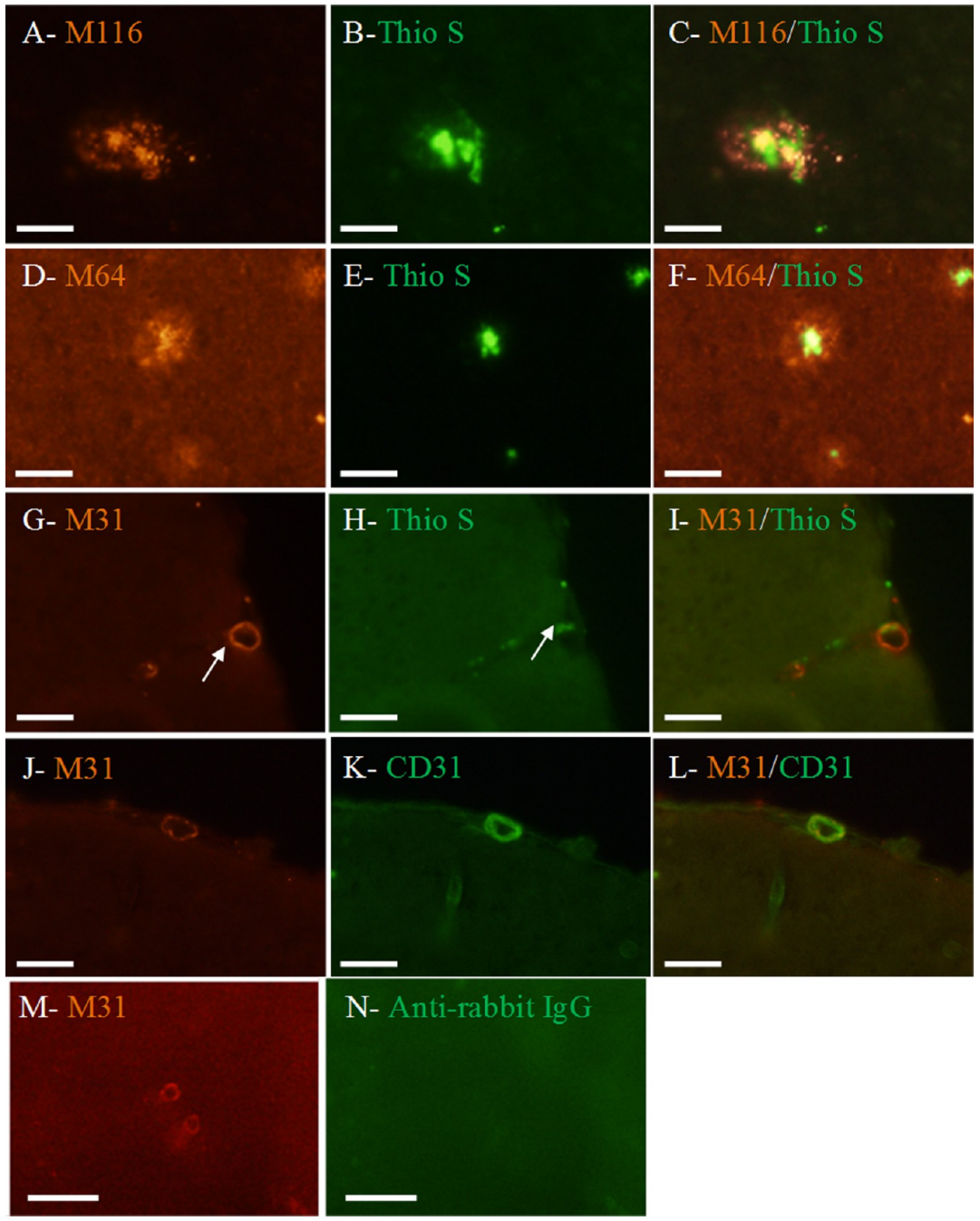

Figure 1. Anti-amyloid-β antibodies bind to cerebral and vascular deposits of Aβ. Representative immunohistochemical staining of 5 month old TgCRND8 brain tissue. (A) M116 binds in the cortex. (B) Thioflavin S positive plaques are detected in the TgCRND8 tissue. (C) Merged images demonstrate that M116 plaques are Thioflavin S positive indicating the deposits to which M116 are binding are composed of Aβ. (D) M64 positive deposits are observed in TgCRND8 brain tissue. (E) Thioflavin S deposits are observed to (F) colocalize with the M64 deposits, confirming these are composed of Aβ. (G) M31 bound to circular shapes (white arrow), indicative of vascular Aβ. (H) M31 deposits are also Thioflavin S positive, and the (I) merged M31/Thioflavin image confirms that the deposits contain Aβ. (J) An M31 deposit stained positive for (K) CD31 and the (L) colocalized image of M31 and CD31 demonstrates that this Aβ deposit is in the vasculature. (M) Tissue stained with M31 and anti-rabbit IgG-Alexa564 shows round, hollow deposits. (N) Tissue stained with anti-rat IgG-Alexa488 does not colocalize with M31 deposits confirming the specificity of CD31 to vasculature. There is no evidence that CD31 positive structures result from nonspecific binding of the secondary antibody. Images (A)−(L) were taken at 20× magnification, and the scale bar is 60 μm. Images (M) and (N) were taken at 10× magnification, and the scale bar is 200 μm.

confirming they were composed of Aβ (Figure 4). Both antibodies remained excellent candidates for live animal imaging of Aβ pathology.

In contrast, no deposits were observed near the injection site of TgCRND8 animals that received intracortical injections of the vascular Aβ-specific antibody M31 (Figure 3E). Similarly, no deposits were found in wild type tissue (Figure 3F). While intracortical injection of M31 antibody did not appear to be a suitable method to detect vascular Aβ, this could be attributed to disruption of the vasculature surrounding the injection site or the inability of M31 to access vascular associated Aβ. Many of the blood vessels observed histologically were in close proximity to

dx.doi.org/10.1021/cn300226q | *ACS Chem. Neurosci.* 2013, 4, 613−623

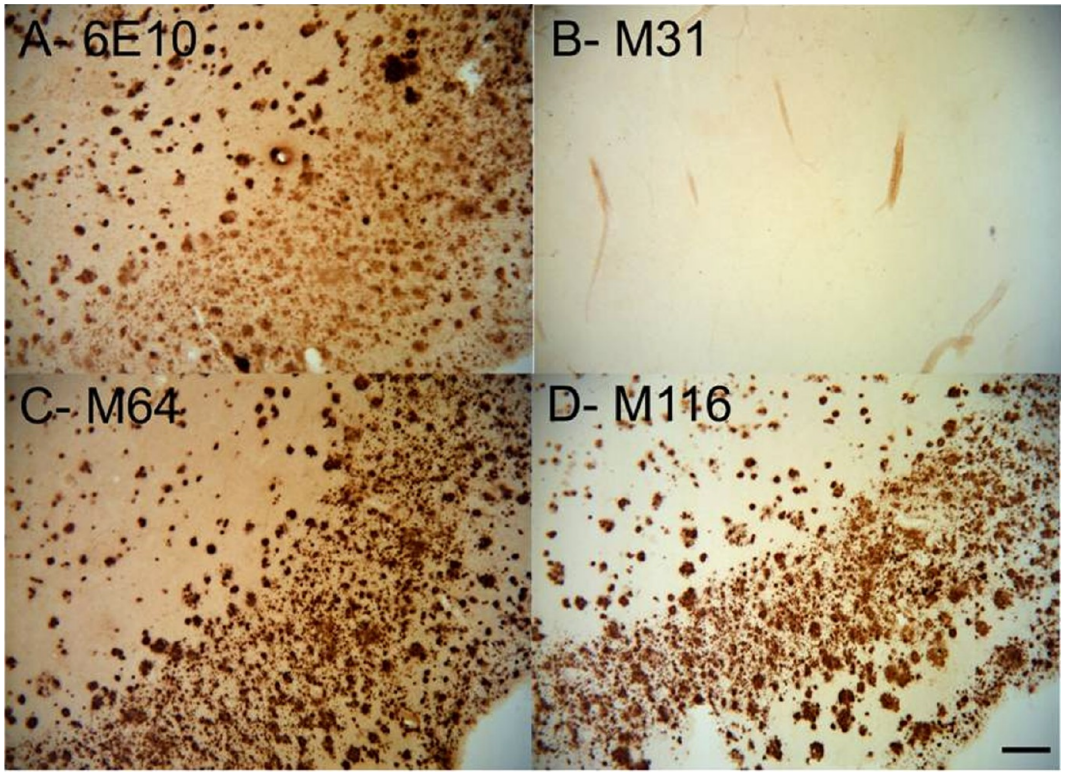

Figure 2. M116, M64, and M31 bind to Aβ deposits in human brain tissue. Human AD brain tissue was taken from Broadmann's area 11, and serial sections were examined with each antibody using immunohistochemistry with DAB staining. (A) Aβ 6E10 reveals extensive plaque deposits and diffuse background staining. (B) M31 binds hollow, branched structures indicative of vascular Aβ which is similar to binding observed in TgCRND8 mouse brain tissue. (C) M64 binds to numerous Aβ plaques, but the background is high which is consistent with results in TgCRND8 mouse brain tissue. (D) M116 binds strongly to Aβ plaques in the parenchyma with very low background. All images are taken at 40× magnification, and the scale bar is 200 μm.

the surface of the brain, which is consistent with previous descriptions of vascular Aβ in TgCRND8 mice.[30] Notwithstanding these results, M31 was still considered a viable candidate for in vivo imaging because an intravenous delivery strategy may overcome the barriers to detection of vascular Aβ observed with intracortical injections.

Intravenous Delivery of PEG-Modified Anti-Amyloid β Antibodies Differentiates TgCRND8 Mice from WT Littermates. All three anti-Aβ antibodies were labeled both with ^{64}Cu, through the intermediate copper chelating moiety DOTA, in order to be used in PET imaging, and with PEG to improve circulation time and promote transport across the BBB. PEG-modification and ^{64}Cu-labeling were verified before injection for each antibody. Tissue was stained with each antibody after PEG-modification and ^{64}Cu-labeling to ensure the chemical modification techniques did not affect binding to the plaques (Supporting Information Figure 1−C). Regions of interest were drawn in the brain using the CT anatomical data (Supporting Information Figure 1D). We did not perform any partial volume corrections because voxel size was approximately 2.9 mm^3 and the region of interest was approximately 450 mm^3. Partial volume error should be minimal because the region of interest was greater than double the spatial resolution of the scanner.[33]

Higher accumulation of M116-PEG-^{64}Cu (targeting parenchymal plaques) in the brain tissue, expressed as percentage of injected dose per gram of tissue (%ID/g), was observed in TgCRND8 mice when compared to wild type mice (Figure 5A). TgCRND8 animals receiving an injection of M64-PEG-^{64}Cu (targeting parenchymal plaques) were indistinguishable from wild type animals at each time point (Figure 5B). Brain concentrations of M31-PEG-^{64}Cu (targeting vascular Aβ) were elevated in the TgCRND8 mice when compared to wild type controls (Figure 5C). In order to examine changes in brain accumulation in the TgCRND8 mice relative to wild type controls, the %ID/g in the TgCRND8 was normalized to the %ID/g in the wild type for each animal and antibody group (Figure 5D). Time was not a significant factor in the three-factor ANOVA (antibody, time, and animal) which limits the statistical conclusions that can be drawn. Notwithstanding, M116 (targeting parenchymal plaques) showed increased accumulation, M64 (targeting parenchymal plaques) remained constant, and M31 (targeting vascular Aβ) showed higher total amounts in the TgCRND8 mouse over the 4 h studied. In order to verify that the PET quantitation was accurate, brain tissue was recovered and quantitated at 4 h with a gamma counter. Percent of injected dose per gram measured with gamma counting in each brain mirrored the PET quantitation (Figure 5E).

A statistical analysis was performed to determine significant effects observed through PET imaging and gamma counting quantitation. Three factor ANOVA (antibody, time, and animal) revealed that antibody ($F = 25.983$, $p < 0.001$) and animal ($F = 90.267$, $p < 0.001$) were significant main effects, indicating that the three different antibodies all affected brain concentrations differently and that TgCRND8 and wild type animals responded differently. Significant two-way interactions were also observed between antibody and animal ($F = 7.338$, $p = 0.002$), indicating that the antibodies performed differently in TgCRND8 and wild type animals. No other main effects, two-way or three-way interactions were significant. The Tukey post-hoc test was performed to look for differences within groups.

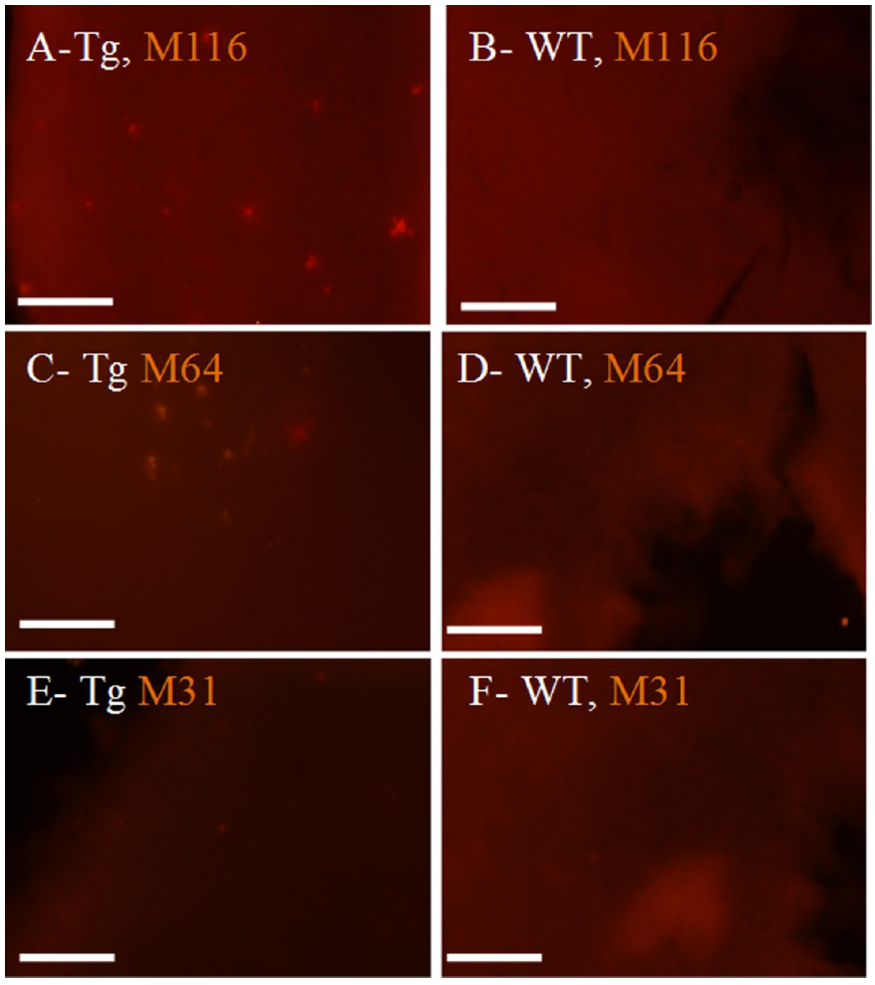

Figure 3. Intracerebral injections of M116 and M64 label Aβ plaques in mouse brain tissue. Labeling of (A) M116 at 4 h after intracortical injection with an anti-rabbit-Alexa548 secondary antibody reveals deposits. (B) Similar labeling of M116 in wild type tissue reveals no deposits. (C) Dense deposits of M64 are observed near the injection site in TgCRND8 animals, while no deposits are found in wild type tissue (D). (E) Intracortical injections of M31 revealed no binding to deposits which is consistent with the vascular plaque labeling. This suggests that intracortical injection of antibodies does not permit the antibodies to cross the vasculature to label the plaques. (F) No labeling of plaques or vasculature was observed in wild type tissue. $N = 3$ for each antibody and animal type. All images are taken at 10× magnification, the scale bar is 200 μm, Tg refers to transgenic TgCRND8 tissue, and WT refers to wild type tissue.

Significant differences in the mean brain %ID/g between TgCRND8 and wild type animals were observed when animals received injections of M116 ($q = 12.186$, $p < 0.001$) and M31 ($q = 12.555$, $p < 0.001$). There was no significant difference between TgCRND8 and wild type mice that received an injection of M64. The statistical analysis confirmed that M116 and M31 are viable antibodies for differentiating between TgCRND8 and wild type mice using noninvasive imaging techniques.

In order to gain greater insight into why M116 (targeting parenchymal plaques) and M31 (targeting vascular Aβ) were able to differentiate between TgCRND8 and wild type mice while M64 (targeting parenchymal plaques) was not, despite positive histological performance of all three antibodies, the biodistribution of each antibody was examined. Three-factor ANOVA was performed on the biodistribution with organ, antibody, and animal as the main factors. Organ ($F = 21.481$, $p < 0.001$), antibody ($F = 10.984$, $p < 0.001$), and animal ($F = 13.530$, $p < 0.001$) were all identified as main effects, and organ and antibody were identified as having a significant interaction ($F = 48.786$, $p < 0.001$) (Figure 6A). Interestingly, significantly less M64-PEG-^{64}Cu was found in the blood of both TgCRND8 and wild type mice than was observed M116-PEG-^{64}Cu ($q = 11.320$, $p < 0.001$) or M31-PEG-^{64}Cu ($q = 10.523$, $p < 0.001$). The inability to differentiate between the TgCRND8 and wild type mice with M64, despite positive histological data, is attributed to these reduced circulation times. Elevated concentrations in the intestines (Figure 6B) were observed for M64 ($q = 10.176$, $p < 0.001$), which appear to be responsible for the decreased blood concentrations. M64 concentrations were not significantly elevated in the liver and kidney (Figure 6C and D). Reduced circulation time of M64 does not appear to be connected to systemic Aβ because the effect was observed in both TgCRND8 and wild type mice. Instead, we propose that differences in the structure or post-translation modifications of the Fc region of M64 are responsible for the altered circulation times. Differences in glycan profiles in the Fc region have been implicated in differing clearance profiles of monoclonal antibodies in humans.[34,35] Specifically, examining the mannose content of the antibodies studied here would be interesting because high-mannose content is correlated with increased circulation.[34,35]

We also observed significantly higher nonspecific background histological staining with M64 when compared to both M116

dx.doi.org/10.1021/cn300226q | ACS Chem. Neurosci. 2013, 4, 613−623

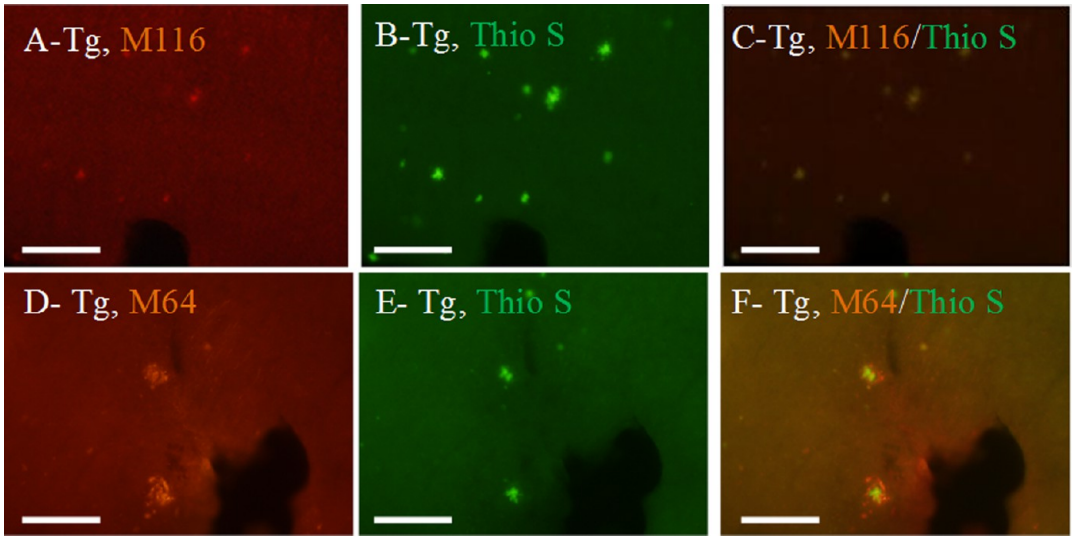

Figure 4. Thioflavin S staining of TgCRND8 tissue that received intracortical injections confirms deposits are composed of Aβ. (A) M116 positive deposits are observed around the injection site. (B) Thioflavin S positive deposits are also observed near the injection site and the merged image (C) shows colocalization of signal confirming M116 deposits are composed of Aβ. (D) M64 positive deposits and (E) Thioflavin S positive deposits are observed around the injection site after intracortical injections. (F) The M64 and Thioflavin S signals show colocalization confirming deposits are composed of Ab. All images are taken at 10× magnification, the scale bar is 200 μm, and Tg refers to transgenic TgCRND8 tissue.

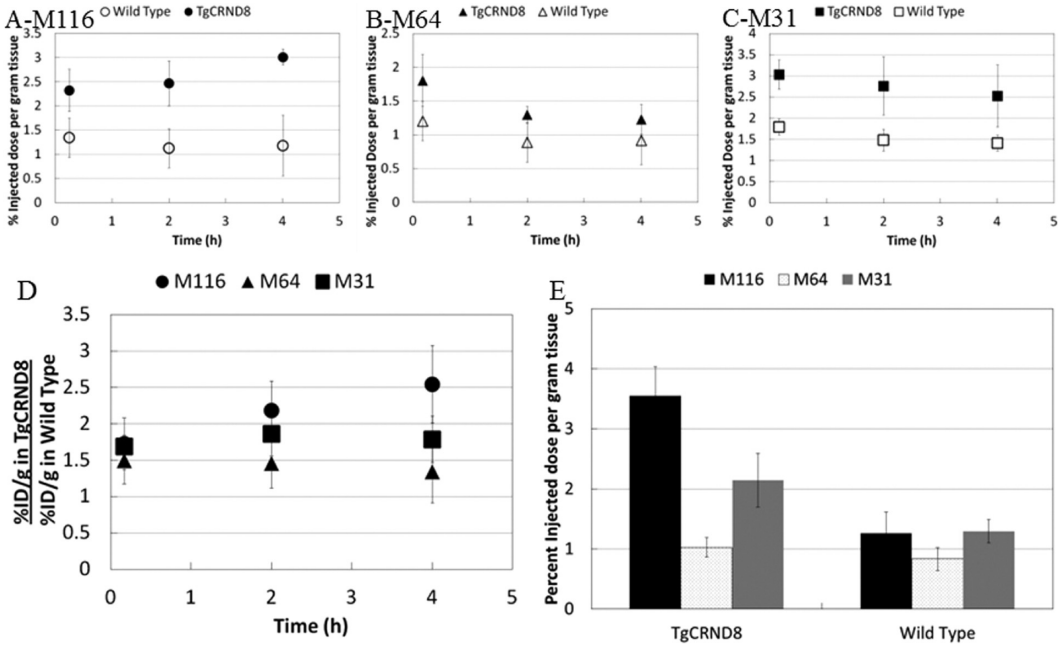

Figure 5. PEG- and ^{64}Cu-modified anti-amyloid-β antibodies M116 and M31 are able to distinguish between TgCRND8 and wild type mice using noninvasive PET imaging. Quantitation of PET images (% of injected dose per gram tissue) in the brain region 5 min, 2 h, and 4 h after intravenous injection of ^{64}Cu-labeled and PEG-modified: (A) M116 shows progressive accumulation of M116 in the TgCRND8 brain vs a lower, constant amount in the WT brain. (B) M64 shows no difference in accumulation between TgCRND8 and wild type mice at any time point. (C) M31 shows greater accumulated amount in TgCRND8 mice than WT, but at a constant amount. (D) Comparing the amounts of M116, M64, and M31 in the TgCRND8 brain relative to the wild type control shows linear increases of M116 while M64 and M31 remain constant of the time period examined. (E) Post-mortem quantitation of brain tissue at 4 h with gamma counting confirms PET quantitation data shown in (A), (B,C) Greater accumulation of M116 and M31 in TgCRND8 vs WT mice, yet no difference in M64. N = 3 for each antibody and animal type.

and M31, which indicates increased nonspecific binding of the M64 to the tissue.[36] In addition to making it more difficult to resolve signal from background noise, enhanced nonspecific binding could be a direct cause of increased removal from circulation. Interestingly, high background staining in the histological environment may be part of a viable strategy to screen out antibodies that will not perform well systemically.

Intravenous Delivery of PEG-Modified Anti-Amyloid β Antibodies Label Parenchymal Plaques and Vascular Deposits of Amyloid β. This study was able to differentiate between TgCRND8 and wild type mice using PET imaging, which was confirmed by post-mortem gamma counting of brain tissue. In order to link the higher accumulation of M116 (targeting parenchymal plaques) and M31 (targeting vascular Aβ)

dx.doi.org/10.1021/cn300226q | ACS Chem. Neurosci. 2013, 4, 613−623

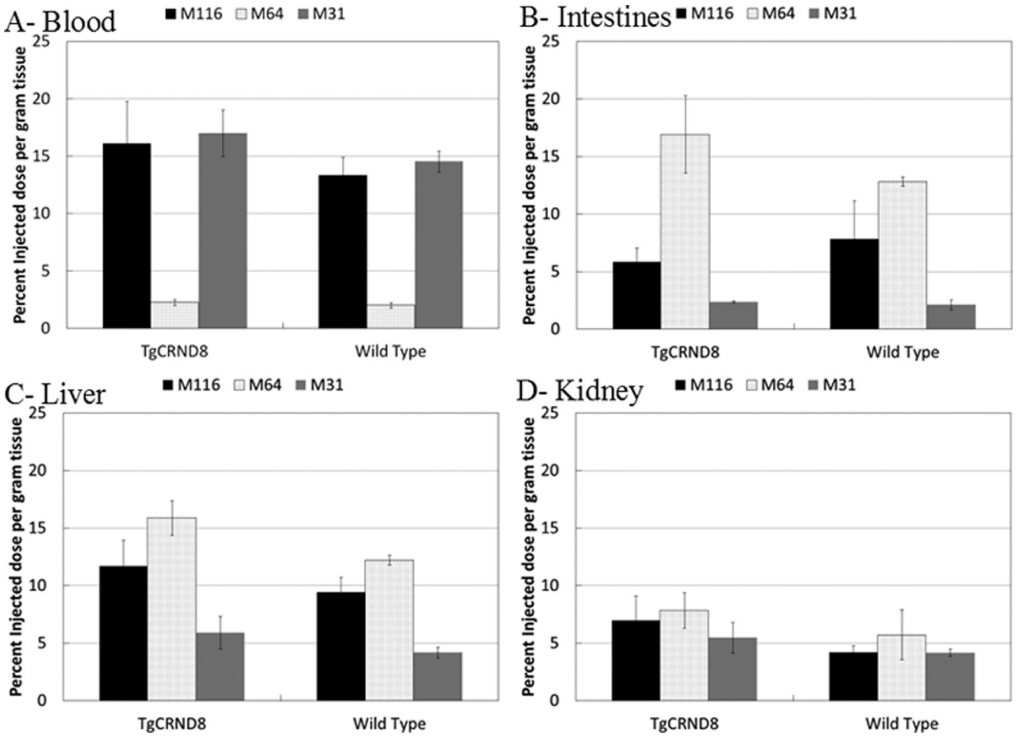

Figure 6. No differences in biodistribution (outside of the brain) were observed between transgenic and wild-type mice: M116 and M31 share similar biodistribution, yet M64 is different. (A) Blood concentrations of M64 are much lower than M116 and M31 in both TgCRND8 and wild type mice at 4 h, demonstrating faster clearance of M64. (B) Large intestine concentrations of M116 and M31 are lower than M64 at 4 h in both TgCRND8 and wild type animals, consistent with the blood concentrations observed. M64 is not significantly elevated in the liver (B) or kidney (C). Higher clearance of M64 appears to be responsible for the reduced blood concentrations. Mean ± standard deviation, $n = 3$.

in the TgCRND8 mouse with Aβ pathology, the brains were sectioned and stained with an anti-rabbit IgG antibody to determine the location of these antibodies. Several deposits were found in the parenchyma of TgCRND8 animals that had received intravenous injections of M116-PEG-^{64}Cu (Figure 7A). These deposits were also Thio-S positive (Figure 7B) and showed colocalization when the images were overlaid (Figure 7C). This confirmed that intravenous delivery of M116-PEG labels parenchymal Aβ plaques and can be used to image Aβ pathology in live animals. In contrast, no deposits were observed in TgCRND8 mice that received intravenous injections of M64-PEG-^{64}Cu, although Thio-S positive plaques were found in these animals (Figure 7D–F). These results are consistent with PET imaging where we were unable to distinguish between TgCRND8 and wild type animals with M64. While M64 bound to Aβ both in ex vivo brain tissue of TgCRND8 mice and the cortex of living TgCRND8 mice when injected directly to the cortex, it is clear that its limited systemic circulation inhibited its ability to cross the BBB and therefore its ultimate utility as a diagnostic. Thus, systemic circulation time and nonspecific tissue binding are two key parameters to consider when choosing an antibody for Aβ targeting.

Circular shaped deposits were found in brain tissue recovered from TgCRND8 mice that received intravenous injections of M31-PEG-^{64}Cu (Figure 7G). Similar to the histological examination of M31 staining in TgCRND8 tissue, these deposits were Thio-S positive (Figure 7H) and overlapped with the M31 signal, which confirms that M31 can detect vascular Aβ deposition (Figure 7I). Although intracortical delivery of M31 did not label vascular Aβ, intravenous delivery of M31-PEG noninvasively detected vascular Aβ in TgCRND8 mice. Tissue from wild type animals was also stained, but no deposits were found (Figure 7J–L). The success of intravenous over intracortical delivery reflects the greater access of the M31 antibody to the vasculature with intravenous. M116 and M64 were successfully able to distinguish between the TgCRND8 and wild type mice, but the Aβ burden was not measured quantitatively. In the future, it will be interesting to use these antibodies to measure Aβ concentrations in the brain.

Intravenous delivery of PEG-modified anti-Aβ antibodies was shown to differentiate TgCRND8 animals from wild type controls using noninvasive PET imaging. Further, two distinct types of Aβ pathology (parenchymal and vascular) were imaged with these antibodies. Despite impressive histological behavior of all three antibodies, only two were successfully translated to noninvasive PET imaging. Post-mortem detection of M116 positive plaques in the brain tissue of TgCRND8 animals that received intravenous injections confirmed that this antibody crossed the BBB in order to gain access to these plaques; however, it is unclear whether M64 and M31 were able to cross the BBB.

These results confirm the principle that individual antibodies have unique behavior and careful screening is necessary to select antibodies that will perform well in a diagnostic and monitoring setting. Moreover, the arrangement of Aβ is highly heterogeneous and interactions between an antibody and Aβ are highly contextual. Elucidating the epitope to which an antibody will bind is not sufficient to identify a diagnostic tool because the availability of the epitope in the dynamic biological environment is as much, if not more important, than the epitope itself. The availability of the epitope depends on the method of delivery. With intravenous injection, longer systemic circulation, diffusion across the BBB and penetration of brain tissue are key parameters that impact ultimate translation.

dx.doi.org/10.1021/cn300226q | *ACS Chem. Neurosci.* 2013, 4, 613–623

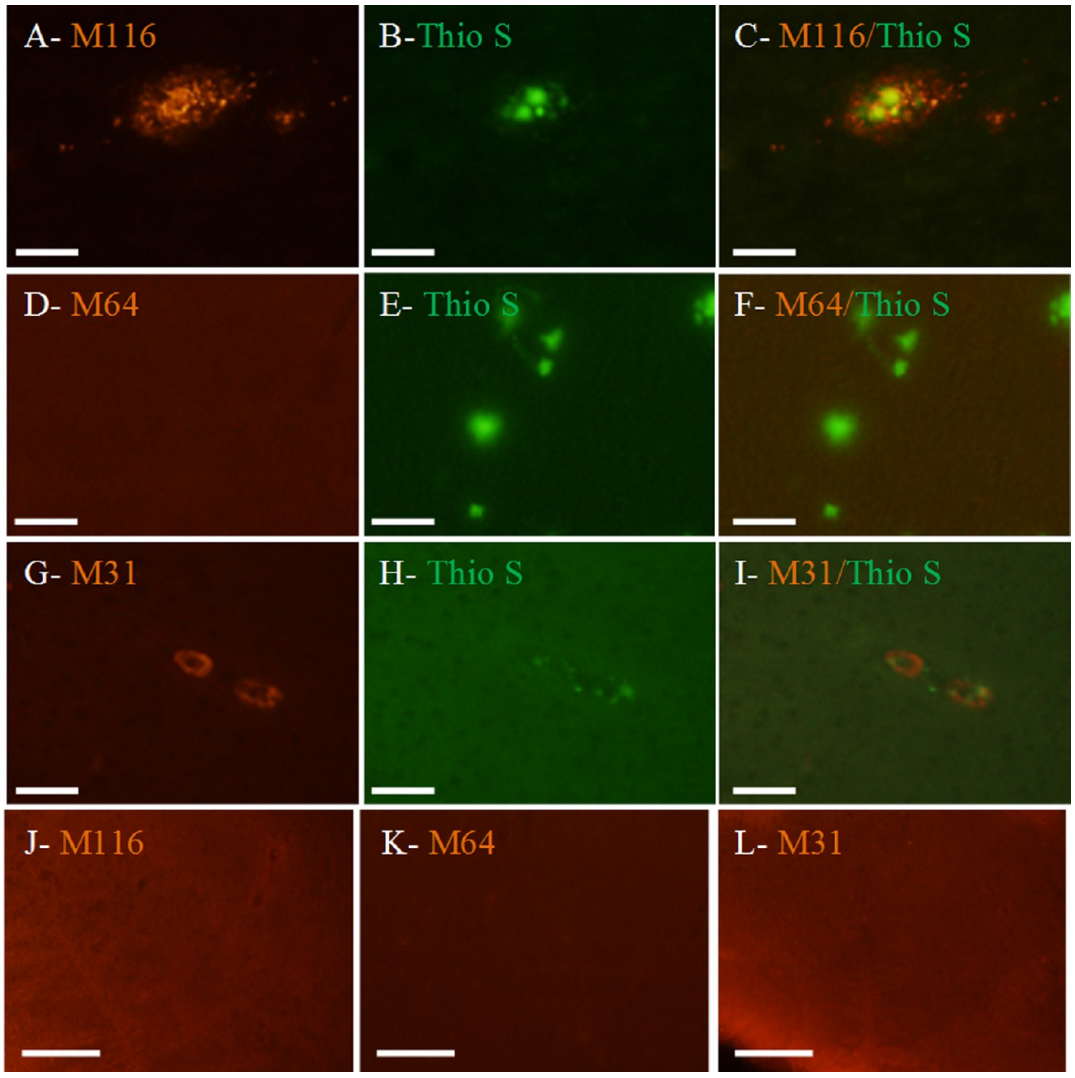

Figure 7. Representative immunohistochemical staining after intravenous delivery of PEG-modified, ^{64}Cu-labeled M116, M64, and M31 confirms M116 and M31 labels Aβ deposits in brain tissue. (A) Staining of PEG-modified M116 with an anti-rabbit-Alexa546 secondary antibody found plaques in the brains of TgCRND8 animals after intravenous injection. (B) Thioflavin S positive plaques were found in the TgCRND8 tissue, and (C) some of the plaques colocalized with M116 deposits. (D) No deposits were found in the TgCRND8 tissue that received intravenous injections of PEG-modified and ^{64}Cu-labeled M64. (E) While this tissue did stain positive for Thioflavin S, (F) no colocalization was evident. (G) Staining of PEG-modified, ^{64}Cu-labeled M31with the anti-rabbit secondary antibody found deposits shaped like blood vessels. (H) Some Thioflavin S positive deposits were found and (I) these deposits localized with the M31 deposit. Tissue sections from wild type tissue were stained with an anti-rabbit IgG-Alexa-564 to detect (J) M116, (K) M64, or (L) M31 after intravenous delivery and PET imaging. No deposits were found in the wild type tissue with any of the three antibodies delivered. Images (A) through (I) were taken at 20× magnification, and the scale bars are 60 μm. Images (J) through (L) were taken at 10× magnification, and the scale bar is 200 μm. N = 3 for each antibody and animal type.

METHODS

Animals. All mouse experiments were reviewed and approved by Institutional Animal Care and Use Committees at the University of Toronto (Toronto, ON) and the University Health Network (Toronto, ON). All rabbit experiments were reviewed and approved by an Institutional Animal Care and Use Committee at the University of California, Irvine. TgCRND8 mice were bred on a 129 background and differentiated from wild type (WT) littermates by RT-PCR analysis of tail tissue DNA. TgCRND8 mice are a widely used and robust model of Aβ deposition and carry the Swedish and Indiana mutations.[37]

Immunohistology with Anti-Aβ Antibodies. Rabbit monoclonal antibodies M31, M64, and M116 were made under contract to Epitomics (Burlingame, CA) using fibrillar Aβ42 as an antigen and immunizing New Zealand white rabbits, as previously described for preparing OC polyclonal serum[38] and monoclonal antibodies M64 and M87.[39]

Approximately 10 000 pools of hybridomas were screened against Aß42 fibrils, prefibrillar oligomers, or monomeric Aβ, and 120 pools having an absorbance at least 3-fold above background in ELISA assays were selected for further analysis. Secondary screening consisted of probing blots of a medium density array of 130 different preparations of fibrils, prefibrillar oligomers, and monomers of Aβ1−42, Aβ1−40, islet amyloid polypeptide (IAPP), polyQ40, overlapping 15 residue peptide segments of Aβ, and amyloid-forming random peptides. Hybridoma pools were also probed by immunohistochemistry on human AD and age-matched control brain tissues. Twenty four pools giving a unique pattern of immunoreactivity on the array or on immunohistochemistry were selected for cloning and further characterization by epitope mapping, immunohistochemistry, Western blotting, and dot blotting. M31 recognizes a discontinuous epitope consisting of residues 3−10 and 22−23 (Hatami, Albay and Glabe, manuscript in preparation). M64 recognizes residues 3−6, but not pyroglutamylated E3 Aβ.[39] M116 recognizes residues 3−9. All 3 antibodies stain high molecular weight

dx.doi.org/10.1021/cn300226q | ACS Chem. Neurosci. 2013, 4, 613−623

Aβ40 or Aβ42 aggregates but not monomer on Western blots (Hatami, Albay, and Glabe, manuscript in preparation).

For histology, 5 month old TgCRND8 animals were sacrificed by CO_2 asphyxiation, and the brains were harvested. Brain tissue was fixed for 24 h in 4% paraformaldehyde and cryo-protected in 30% sucrose for 24 h. Brain tissue was snap frozen in dry ice cooled isopentane and cut into 20 μm thick sections using a Leica cryostat. Brain sections were post fixed for 5 min in 4% paraformaldehyde, washed three times with phosphate buffered saline (PBS), and blocked for 1 h in 1% bovine albumin (Sigma-Aldrich). Anti-Aβ antibodies raised toward parenchymal aggregated plaques (M64 and M116) in rabbits were incubated on brains sections for 12 h at room temperature (PBS, 1:50 dilution) and sections were washed three times with PBS. Goat anti-rabbit IgG-Alexa-548 (Invitrogen, PBS, 1:200 dilution) was incubated for 2 h at room temperature and washed 4 times with PBS. Selected sections were counter stained with 1% Thioflavin-S, a well-established stain for Aβ aggregates[40] (Sigma-Aldrich), for 8 min, followed by 80% ethanol for 8 min twice, 95% ethanol once, and three washes with distilled water. Images were viewed under a fluorescent microscope with a FITC and TRITC filter.

To stain for CD31, the antigen was retrieved through digestion with 0.1 mg/mL Proteinase K (Sigma-Aldrich) for 10 min. A rat anti-mouse CD31 primary antibody (BD# 550274, PBS, 1:10 dilution) was incubated overnight at room temperature. After washing three times with PBS, a goat anti-rat IgG-Alexa-488 secondary antibody (Invitrogen, PBS, 1:200 dilution) was incubated for 2 h at room temperature.

Immunohistology after Intracortical Injection of Anti-Aβ Antibodies. Five month old TgCRND8 and wild type littermates were anesthestized with isoflurance (5% induction, 3% maintenance) and positioned in a stereotactic device (Kopf) and the skull was exposed with a small incision. Two holes were drilled in the skull at rostal 1 mm and lateral ±2 mm relative to bregma. A volume of 0.5 μL of each antibody (M116, M64, and M31) was separately injected into the left cortex of TgCRND8 and wildtype animals (n = 3 for each antibody and animal type) with a 10 μL Hamilton syringe and 26 gauge needle and 45° bevel tip. The needle was lowered 1 mm from the top of the skull into the left cortex, and the antibody was injected at 0.1 μL/min, left in place for 10 min, and removed at a rate of 0.2 mm/min. An internal control was performed in each animal by injecting saline into the right cortex of each animal. The incision was closed with sutures, and animals were given an injection of ketoprofen (as an analgesic) and saline and allowed to recover. At 4 h after injection, animals were sacrificed by CO_2 asphyxiation and the brains recovered. Brain tissue was treated as described in the above immunohistology methods except tissue was cut into 100 μm sections and only stained with the secondary antibody (the primary antibody was injected) as described above.

Modification of Antibodies with Poly(ethylene glycol) and DOTA. Each anti-Aβ antibody (M116, M64, M31) was labeled with the copper chelating macrocyclic 1,4,7,10-tetraazacyclododecane-1,4,7,10-tetraacetic acid mono(*N*-hydroxysuccinimide ester) (DOTA-NHS) and a 10 kDa PEG mono(*N*-hydroxysuccinimide ester) chain (Rapp Polymere) through NHS coupling chemistry, as previously described.[28] Antibodies were prepared in PBS (500 μg/mL) and incubated with 10 times molar excess of 1 mg/mL PEG-NHS and DOTA-NHS for 4 h at room temperature. Antibody-PEG-DOTA conjugates were purified with four washes in a centrifugal filtration unit (Amicon Ultra-0.5 mL centrifugal 100 kDa MWCO filter units, Millipore). Successful modification with PEG was verified by sodium dodecyl sulfate polyacrylamide gel electrophoresis. A nonreducing 5% acrylamide gel was resolved for 1 h at 100 V. Protein was visualized with SimplyBlue SafeStain (Invitrogen), and PEG was visualized using a barium iodine stain previously described.[41]

^{64}Cu was synthesized the day prior to radiolabeling at the Centre d'imagerie moleculaire de Sherbrooke (CIMS, Sherbrooke, QC). Antibody-PEG-DOTA conjugates were radiolabeled using a previously reported protocol.[28] Briefly antibody-PEG-DOTA was incubated with 5mCi of ^{64}Cu at room temperature in PBS for 2 h. Radiolabeled antibody-PEG-DOTA-^{64}Cu was purified from excess ^{64}Cu with four washes in a centrifugal filtration (Amicon Ultra-0.5 mL centrifugal 30 kDa MWCO filter units, Millipore). A volume of 0.5 μL of the purified conjugate was placed on an Instant Thin Layer Chromatography (iTLC) sheet (iTLC-SG, Pall) and resolved in 0.1 M, pH5 citrate buffer. iTLC sheets were visualized and quantified with a Cyclone Plus Phosphor Imager device (Perkin-Elmer). Conjugates were at least 95% pure before injected in vivo. Conjugates were checked for bioactivity by repeating the immunohistology methods described above.

Intravenous Injection and Positron Emission Tomography of Radiolabeled Antibodies. Twenty-five μg of M116-PEG-^{64}Cu, M64-PEG-^{64}Cu or M31-PEG-^{64}Cu was administered to 5 month old TgCRND8 (n = 3) and WT littermates (n = 3) by intravenous tail vein injection. Dosage was calculated by measuring the activity in the administration syringe before and after injection with a dose calibrator (CRC-15R, Capintec). Animals received a minimum of 50 μCi. After injection, animals were anaesthetized with isoflurane (5% induction, 3% maintenance) and placed on a PET imaging bed (Minnerve). Animals were imaged with a microPET (Siemens Micro PET Focus 220) at the Spatiotemporal Targeting and Amplification of Radiation Response (STTARR) Innovation Centre (University Health Network, Toronto, ON) for 15 min after injection and at 2 and 4 h. In order to provide spatial anatomical data, animals were immediately transferred to a microCT (GE Locus Ultra microCT) for a 15 s computed tomography scan at the same facility. Animals recovered in between scans and had access to food, water and enrichment. At 4 h, animals were sacrificed by cardiac puncture under anesthesia. All organs were collected, weighed and the radioactive ^{64}Cu dose measured in a gamma counter (Wallac Wizard 3, Perkin-Elmer). The percent injected dose per gram of tissue was calculated using a standard curve of ^{64}Cu (cross-calibrated to the dose calibrator used to calculate the injected dose).

Reconstruction and Analysis of PET Images. PET scans were reconstructed as a single frame with a 128 × 128 × 95 matrix (voxel size 1.9 × 1.9 × 0.8 mm^3) using an iterative reconstruction method (OSEM3D/MAP, 2 subsets of 9 iterations). CT scans were reconstructed with a 256 × 256 × 680 image matrix (voxel size 154 × 154 × 154 μm^3). PET and CT data sets were manually fused using Inveon Research Workplace (Siemens). Intensity on the PET images was increased to reveal the animals shape and allow the head, body, arms, and legs to be matched to the CT image. The CT images were used to provide spatial/structural information for locations of the brain in the PET images. The region of interest was drawn in the brain and the amount of ^{64}Cu quantitated as a mean percent injected dose per gram of tissue (%ID/g) at each time point. Quantitation of these small volumes was possible because the skull provided important spatial information that allowed the brain to be clearly differentiated from the other tissues. Each image was fused and quantified three times to reduce bias due to fusing error. Radioactive decay was corrected for in all %ID/g tissue measurements reported using a standard exponential decay formula.

Immunohistology after Intravenous Injection of Anti-Aβ Antibodies. After gamma counting, brain tissue was placed into 4% paraformaldehyde for 1 week. After the ^{64}Cu had decayed, brains were transferred to 30% sucrose for 24 h. Brain tissue was stained with an anti-rabbit IgG-Alexa-548 secondary antibody as described in the immunohistology methods to determine if the intravenous injection of anti-Aβ antibodies resulted in labeling of Aβ deposits.

Statistics. Data are plotted as mean ± standard deviation of the mean. Data was subjected to three-factor analysis of variance (ANOVA) followed by a Tukey posthoc test for comparisons between means. Relevant main effects and interactions are presented along with F- and p-values. P values of <0.05 were regarded as significant. All tests were performed using statistical software SigmaPlot 11.0.

■ ASSOCIATED CONTENT

Supporting Information

Additional figures as described in the text. This material is available free of charge via the Internet at http://pubs.acs.org.

■ AUTHOR INFORMATION

Funding

D.M. acknowledges the Vanier Canada Graduate Scholarship programme, and M.J.C. acknowledges the Ontario Neurotrauma

Foundation postdoctoral fellowship. Work was funded by the Natural Sciences and Engineering Research Council of Canada (to M.S.S.), National Institutes of Health (NIH AG33069, to C.G.), Cure Alzheimer Fund (to C.G.), and a Firefly Foundation Grant (to Drs. Paul Fraser and Peter Hyslop).

Notes

The authors declare no competing financial interest.

■ ACKNOWLEDGMENTS

The authors gratefully acknowledge the advice of Drs. Paul Fraser and Peter Hyslop and technical expertise of Rosemary Ahrens (Centre for Research in Neurodegenerative Diseases, University of Toronto) for assistance with the TgCRND8 mouse model, and Deborah Scollard for her imaging expertise.

■ REFERENCES

(1) Hampel, H., Prvulovic, D., Teipel, S., Jessen, F., Luckhaus, C., Froliche, L., Riepe, M. W., Dodel, R., Leyhe, T., Bertram, L., Hoffmann, W., Faltraco, F., and German Task Force Alzheimer's, D. (2011) The future of Alzheimer's disease: The next 10 years. *Prog. Neurobiol. 95*, 718−728.

(2) Brookmeyer, R., Johnson, E., Ziegler-Graham, K., and Arrighi, H. M. (2007) Forecasting the global burden of Alzheimer's disease. *Alzheimer's Dementia 3*, 186−191.

(3) Holtzman, J. L. (2010) Are We Prepared to Deal With the Alzheimer's Disease Pandemic? *Clin. Pharmacol. Ther. 88*, 563−565.

(4) McKhann, G. M., Knopman, D. S., Chertkow, H., Hyman, B. T., Jack, C. R., Jr, Kawas, C. H., Klunk, W. E., Koroshetz, W. J., Manly, J. J., Mayeux, R., Mohs, R. C., Morris, J. C., Rossor, M. N., Scheltens, P., Carrillo, M. C., Thies, B., Weintraub, S., and Phelps, C. H. (2011) The diagnosis of dementia due to Alzheimer's disease: Recommendations from the National Institute on Aging-Alzheimer's Association work-groups on diagnostic guidelines for Alzheimer's disease. *Alzheimer's Dementia 7*, 263−269.

(5) Tanzi, R. E., and Bertram, L. (2005) Twenty Years of the Alzheimer's Disease Amyloid Hypothesis: A Genetic Perspective. *Cell 120*, 545−555.

(6) Ballatore, C., Lee, V. M. Y., and Trojanowski, J. Q. (2007) Tau-mediated neurodegeneration in Alzheimer's disease and related disorders. *Nat. Rev. Neurosci. 8*, 663−672.

(7) Selkoe, D. J. (2008) Biochemistry and molecular biology of amyloid beta-protein and the mechanism of Alzheimer's disease. In *Handbook of clinical neurology* (Vinken, P. J., and Bruyn, G.W., Eds.), Vol. *89*, pp 245−260.

(8) Carter, M. D., Simms, G. A., and Weaver, D. F. (2010) The Development of New Therapeutics for Alzheimer's Disease. *Clin. Pharmacol. Ther. 88*, 475−486.

(9) Morse, D. L., and Gillies, R. J. (2010) Molecular imaging and targeted therapies. *Biochem. Pharmacol. 80*, 731−738.

(10) Shankar, G. M., Li, S. M., Mehta, T. H., Garcia-Munoz, A., Shepardson, N. E., Smith, I., Brett, F. M., Farrell, M. A., Rowan, M. J., Lemere, C. A., Regan, C. M., Walsh, D. M., Sabatini, B. L., and Selkoe, D. J. (2008) Amyloid-beta protein dimers isolated directly from Alzheimer's brains impair synaptic plasticity and memory. *Nat. Med. 14*, 837−842.

(11) Bernstein, S. L., Dupuis, N. F., Lazo, N. D., Wyttenbach, T., Condron, M. M., Bitan, G., Teplow, D. B., Shea, J. E., Ruotolo, B. T., Robinson, C. V., and Bowers, M. T. (2009) Amyloid-beta protein oligomerization and the importance of tetramers and dodecamers in the aetiology of Alzheimer's disease. *Nat. Chem. 1*, 326−331.

(12) Rabinovici, G. D., F., A. J., O'Neil, J. P., Racine, C. A., Mormino, E. C., Baker, S. L., Chetty, S., Patel, P., Pagliaro, T. A., Klunk, W. E., Mathis, C. A., Rosen, H. J., Miller, B. L., and Jagust., W. J. (2007) 11C-PIB PET imaging in Alzheimer disease and frontotemporal lobar degeneration. *Neurology 68*, 1205−1212.

(13) Nordberg, A. (2004) PET imaging of amyloid in Alzheimer's disease. *Neurology 3*, 519−527.

(14) Cairns, N. J., Ikonomovic, M. D., Benzinger, T., Storandt, M., Fagan, A. M., Shah, A. R., Reinwald, L. T., Carter, D., Felton, A., Holtzman, D. M., Mintun, M. A., Klunk, W. E., and Morris, J. C. (2009) Absence of Pittsburgh Compound B Detection of Cerebral Amyloid beta in a Patient With Clinical, Cognitive, and Cerebrospinal Fluid Markers of Alzheimer Disease. *Arch. Neurol. 66*, 1557−1562.

(15) Nordberg, A. (2004) PET imaging of amyloid in Alzheimer's disease. *Lancet Neurol. 3*, 519−527.

(16) Vasilevko, V., Pop, V., Kim, H. J., Saing, T., Glabe, C. C., Milton, S., Barrett, E. G., Cotman, C. W., Cribbs, D. H., and Head, E. (2010) Linear and conformation specific antibodies in aged beagles after prolonged vaccination with aggregated Abeta. *Neurobiol. Dis. 39*, 301−310.

(17) Habicht, G., Haupt, C., Friedrich, R. P., Hortschansky, P., Sachse, C., Meinhardt, J., Wieligmann, K., Gellermann, G. P., Brodhun, M., Götz, J., Halbhuber, K.-J., Röcken, C., Horn, U., and Fändrich, M. (2007) Directed selection of a conformational antibody domain that prevents mature amyloid fibril formation by stabilizing Aβ protofibrils. *Proc. Natl. Acad. Sci. U.S.A. 104*, 19232−19237.

(18) Kayed, R., and Glabe, C. G. (2006) Conformation-Dependent Anti-Amyloid Oligomer Antibodies, In *Methods in Enzymology* (Indu, K., and Ronald, W., Eds.), pp 326−344, Academic Press.

(19) Glabe, C. G. (2004) Conformation-dependent antibodies target diseases of protein misfolding. *Trends Biochem. Sci. 29*, 542−547.

(20) Poduslo, M. R., Holasek, S. S., Ramirez-Alvarado, M., Kandimalla, K. K., Gilles, E. J., Curran, G. L., and Wengenack., T. M. (2007) In vivo targeting of antibody fragments to the nervous system for Alzheimer's disease immunotherapy and molecular imaging of amyloid plaques. *J. Neurochem. 102*, 420−433.

(21) Ramakrishnan, M., M. W., T., Kandimalla, K. K., Curran, G. L., Gilles, E. J., Ramirez-Alvarado, M., Lin, J., Garwood, M., Rack, C. R., and Poduslo., J. F. (2007) Selective contrast enhancement of individual Alzheimer's disease amyloid plaques using a polyamine and Gd-DOTA conjugated antibody fragment against fibrillar Abeta42 for magnetic resonance molecular imaging. *Pharm. Res. 25*, 1861−1872.

(22) Koffie, R. M., Farrar, C. T., Saidi, L. J., William, C. M., Hyman, B. T., and Spires-Jones, T. L. (2011) Nanoparticles enhance brain delivery of blood-brain barrier-impermeable probes for in vivo optical and magnetic resonance imaging. *Proc. Natl. Acad. Sci. U.S.A. 108*, 18837−18842.

(23) Ni, F., Jiang, L., Yang, R., Chen, Z., Qi, X., and Wang, J. (2012) Effects of PEG length and iron oxide nanoparticles size on reduced protein adsorption and non-specific uptake by macrophage cells. *J. Nanosci. Nanotechnol. 12*, 2094−2100.

(24) Veronese, F. M. (2001) Peptide and protein PEGylation: a review of problems and solutions. *Biomaterials 22*, 405−417.

(25) Bjugstad, K. B., Redmond, D. E., Jr., Lampe, K. J., Kern, D. S., Sladek, J. R., Jr., and Mahoney, M. J. (2008) Biocompatibility of PEG-based hydrogels in primate brain. *Cell Transplant. 17*, 409−415.

(26) Greenwald, R. B. (2001) PEG drugs: an overview. *J. Controlled Release 74*, 159−171.

(27) Kim, H. R., Gil, S., Andrieux, K., Nicolas, V., Appel, M., Chacun, H., Desmaele, D., Taran, F., Georgin, D., and Couvreur, P. (2007) Low-density lipoprotein receptor-mediated endocytosis of PEGylated nanoparticles in rat brain endothelial cells. *Cell. Mol. Life Sci. 64*, 356−364.

(28) McLean, D., Cooke, M. J., Wang, Y., Green, D., Fraser, P. E., St. George-Hyslop, P., and Shoichet, M. S. (2012) Anti-Amyloid-β -mediated Positron Emission Tomography Imaging in Alzheimer's Disease Mouse Brains. *PLoS One 7*, e51958.

(29) Boche, D., Zotova, E., Weller, R. O., Love, S., Neal, J. W., Pickering, R. M., Wilkinson, D., Holmes, C., and Nicoll, J. A. R. (2008) Consequence of Aβ immunization on the vasculature of human Alzheimer's disease brain. *Brain 131*, 3299−3310.

(30) Van Vickle, G. D., Esh, C. L., Kalback, W. M., Patton, R. L., Luehrs, D. C., Kokjohn, T. A., Fifield, F. G., Fraser, P. E., Westaway, D., McLaurin, J., Lopez, J., Brune, D., Newel, A. J., Poston, M., Beach, T. G., and Roher, A. E. (2007) TgCRND8 amyloid precursor protein transgenic mice exhibit an altered gamma-secretase processing and an

aggressive, additive amyloid pathology subject to immunotherapeutic modulation. *Biochemistry 46*, 10317−10327.
(31) Arends, Y., Duyckaerts, C., Rozemuller, J., Eikelenboom, P., and Hauw, J. (2000) Microglia, amyloid and dementia in alzheimer disease: a correlative study. *Neurobiol. Aging 21*, 39−47.
(32) McLean, D., Cooke, M. J., Wang, Y., Fraser, P., George-Hyslop, P. S., and Shoichet, M. S. (2012) Targeting the amyloid-β antibody in the brain tissue of a mouse model of Alzheimer's disease. *J. Controlled Release 159*, 302−308.
(33) Aston, J. A. D., Cunningham, V. J., Asselin, M. C., Hammers, A., Evans, A. C., and Gunn, R. N. (2002) Positron Emission Tomography Partial Volume Correction: Estimation and Algorithms. *J. Cereb. Blood Flow Metab. 22*, 1019−1034.
(34) Chen, X., Liu, Y. D., and Flynn, G. C. (2009) The effect of Fc glycan forms on human IgG2 antibody clearance in humans. *Glycobiology 19*, 240−249.
(35) Goetze, A. M., Liu, Y. D., Zhang, Z., Shah, B., Lee, E., Bondarenko, P. V., and Flynn, G. C. (2011) High-mannose glycans on the Fc region of therapeutic IgG antibodies increase serum clearance in humans. *Glycobiology 21*, 949−959.
(36) Skliris, G. P., Parkes, A. T., Limer, J. L., Burdall, S. E., Carder, P. J., and Speirs, V. (2002) Evaluation of seven oestrogen receptor β antibodies for immunohistochemistry, western blotting, and flow cytometry in human breast tissue. *J. Pathol. 197*, 155−162.
(37) Chishti, M. A., Yang, D. S., Janus, C., Phinney, A. L., Horne, P., Pearson, J., Strome, R., Zuker, N., Loukides, J., French, J., Turner, S., Lozza, G., Grilli, M., Kunicki, S., Morissette, C., Paquette, J., Gervais, F., Bergeron, C., Fraser, P. E., Carlson, G. A., St George-Hyslop, P., and Westaway, D. (2001) Early-onset amyloid deposition and cognitive deficits in transgenic mice expressing a double mutant form of amyloid precursor protein 695. *J. Biol. Chem. 276*, 21562−21570.
(38) Kayed, R., Head, E., Sarsoza, F., Saing, T., Cotman, C., Necula, M., Margol, L., Wu, J., Breydo, L., Thompson, J., Rasool, S., Gurlo, T., Butler, P., and Glabe, C. (2007) Fibril specific, conformation dependent antibodies recognize a generic epitope common to amyloid fibrils and fibrillar oligomers that is absent in prefibrillar oligomers. *Mol. Neurodegener. 2*, 18.
(39) Nussbaum, J. M., Schilling, S., Cynis, H., Silva, A., Swanson, E., Wangsanut, T., Tayler, K., Wiltgen, B., Hatami, A., Ronicke, R., Reymann, K., Hutter-Paier, B., Alexandru, A., Jagla, W., Graubner, S., Glabe, C. G., Demuth, H. U., and Bloom, G. S. (2012) Prion-like behaviour and tau-dependent cytotoxicity of pyroglutamylated amyloid-beta. *Nature 485*, 651−655.
(40) Espargaro, A., Sabate, R., and Ventura, S. (2012) Thioflavin-S staining coupled to flow cytometry. A screening tool to detect in vivo protein aggregation. *Mol. BioSyst. 8*, 2839−2844.
(41) Hardy, E., Ramón, J., Saez, V., Báez, R., Tejeda, Y., and Ruiz, A. (2008) Detection of PEGylated proteins in polyacrylamide gels by reverse staining with zinc and imidazole salts. *Electrophoresis 29*, 2363−2371.